ACS APPLIED MATERIALS & INTERFACES

Letter

www.acsami.org

Conducting Shrinkable Nanocomposite Based on Au-Nanoparticle Implanted Plastic Sheet: Tunable Thermally Induced Surface Wrinkling

Francesco Greco,*[,†] Andrea Bellacicca,[‡] Mauro Gemmi,[§] Valentina Cappello,[§] Virgilio Mattoli,[†] and Paolo Milani*[,‡]

[†]Center for Micro-BioRobotics @SSSA, Istituto Italiano di Tecnologia, Viale Rinaldo Piaggio 34, 56025 Pontedera, Italy

[‡]CIMAINA and Dipartimento di Fisica, Università degli Studi di Milano, via Celoria 16, 20133 Milano, Italy

[§]Center for Nanotechnology Innovation@NEST, Istituto Italiano di Tecnologia, Piazza San Silvestro 12, 56127 Pisa, Italy

Supporting Information

ABSTRACT: A thermally shrinkable and conductive nanocomposite material is prepared by supersonic cluster beam implantation (SCBI) of neutral Au nanoparticles (Au NPs) into a commercially available thermo-retractable polystyrene (PS) sheet. Micronanowrinkling is obtained during shrinking, which is studied by means of SEM, TEM and AFM imaging. Characteristic periodicity is determined and correlated with nanoparticle implantation dose, which permits us to tune the topographic pattern. Remarkable differences emerged with respect to the well-known case of wrinkling of bilayer metal−polymer. Wrinkled composite surfaces are characterized by a peculiar multiscale structuring that promises potential technological applications in the field of catalytic surfaces, sensors, biointerfaces, and optics, among others.

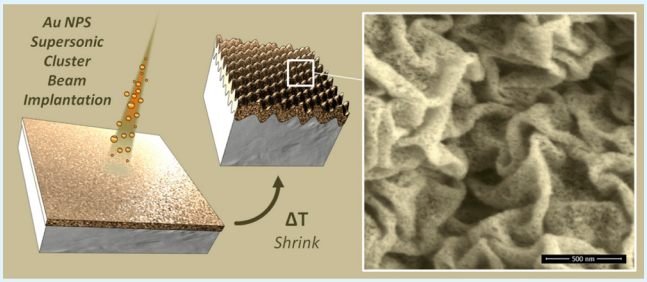

KEYWORDS: *surface wrinkling, metal NPs, implantation, nanocomposite, pattern, shrink, buckling*

Surface wrinkling is a self-organization phenomenon in which the surface of a stiff plate (or a "skin") coupled to a soft elastic substrate rearranges in wavy topographical features (wrinkles) when subjected to compressive stress exceeding a certain critical threshold.[1−3] The wavelength and the amplitude of the surface periodic structures depend on the intrinsic mechanical properties of the materials composing the bilayer system, on their thickness and on the amount of strain.[4] Surface wrinkling, driven by mechanical instability, is widely observed in natural systems such as human skin or fruits and leaves of plants, the physical mechanisms underlying it have been widely investigated.[5,6] The exploitation of surface wrinkling for the micro- and nanopatterning of surfaces has also been demonstrated recently as in view of different applications,[7,8] as well as a metrology technique for the characterization of the mechanical properties of thin films.[9] Microwrinkling has been demonstrated on the surface of shrinkable thermoplastics (e.g., commercially available films of thermoretractable polystyrene (PS) or polyolefins) subjected to heating. Wrinkled metallic surfaces obtained by depositing a metal film on shrinkable thermoplastics were reported by Khine and co-workers[10] and used as substrates for fluorescence enhancement.[11,12] Micro- and nanowrinkling was also successfully applied for the culturing and alignment of embryonic stem cells[13] and for the development of superhydrophobic and antibacterial surfaces.[14] Wrinkling of thermoretractable PS with a Pd thin film was used by Greco et al. for the development of a low-cost resistive hydrogen sensor.[15] The same group then reported wrinkling of the conductive polymer PEDOT:PSS on top of PS to obtain smart biointerfaces able to direct cell alignment and provide a means for their electrical/electrochemical stimulation.[16] Recently, a wrinkled surface composed of a thin (100 nm) film of pyrite (FeS_2) nanocrystals deposited on shrink-wrap film by spray coating has been presented as catalytic surface via Fenton chemistry for oxidative footprinting analysis of proteins.[17]

Polymer−metal nanocomposites are considered key ingredients for the fabrication of electronic skin, soft robots and smart touch sensors,[18,19] thus the micro- and nanopatterning of their surfaces would be highly beneficial for these applications; however, surface wrinkling of polymer nanocomposites embedding nanoparticles has not been demonstrated so far. This is mainly due to the intrinsic difficulty in producing nanocomposite systems able to shrink or to embed nanoparticles in preformed shrinkable materials without significantly altering their properties.

Received: January 27, 2015
Accepted: March 26, 2015
Published: March 26, 2015

DOI: 10.1021/acsami.5b00825
ACS Appl. Mater. Interfaces 2015, 7, 7060−7065

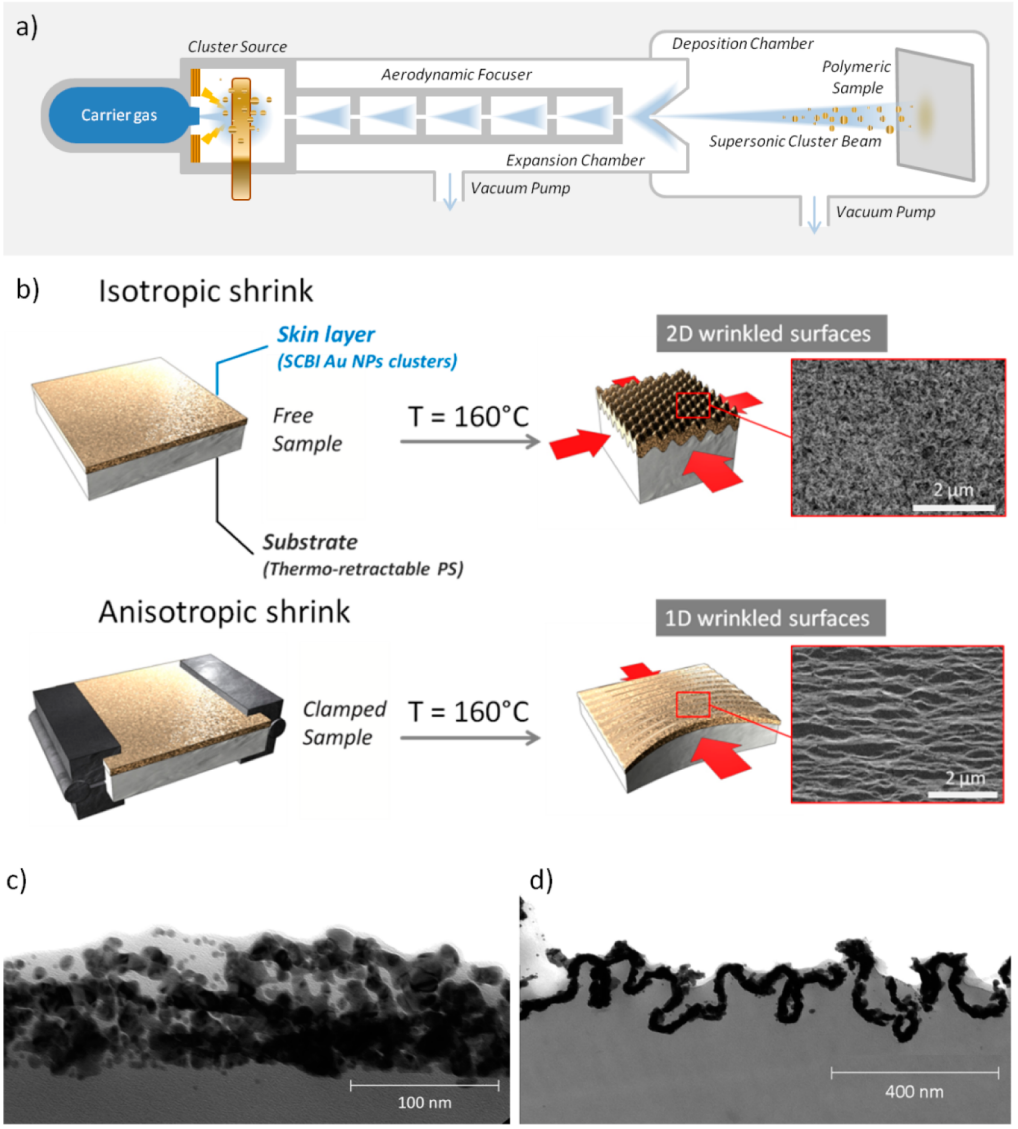

Figure 1. (a) Schematic view of AuNPs implantation process with SCBI apparatus. Neutral Au NPs (cluster size range 3−10 nm) are produced in a cluster source and accelerated by a carrier gas in a supersonic expansion. After being focused by a series of aerodynamic lenses the clusters beam impacts on the surface of a thermo-retractable PS sheet. (b) Scheme of thermally induced shrink processes for obtaining 1D and 2D wrinkling. TEM images of cross sections of AuNPs/PS composite (eq thickness, t_{eq} = 15 nm) cut by an ultramicrotome: (c) flat (not shrunk) sample; (d) 1D wrinkled sample.

Here we present a thermally shrinkable nanocomposite material obtained by supersonic cluster beam implantation (SCBI) of neutral Au nanoparticles (Au NPs) into a commercially available thermo-retractable polystyrene (PS) sheet (Polyshrink). By SCBI neutral metallic clusters are supersonically accelerated toward the surface of a target polymer film (Figure 1a).[20] The cluster kinetic energy is sufficient for implantation, while avoiding electrical charging and thermally induced modification of the polymeric substrate.[21] SCBI of metal nanoparticles in elastomers or thermoplastic polymers has been recently demonstrated as an efficient method for the microfabrication of flexible and stretchable conductive circuits and electrodes.[20−22]

After the implantation of Au nanoparticles (size distribution 3−10 nm) into the thermo-retractable polystyrene to produce an electrical conducting nanocomposite "skin" of AuNPs/PS (Figure 1c), we investigated surface wrinkling of the nanocomposite induced by thermal shrinking of the material at 40% of its original lateral dimension (Figure 1b). Isotropic surface wrinkling (biaxial 2D) was obtained on samples by inducing thermal shrinking at T = 160 °C for 6 min. By mechanically confining the shrinking of the material, we imposed the alignment of wrinkles along a given direction, creating anisotropic (uniaxially aligned, 1D) surface patterns (Figure1b).

We produced different nanocomposite samples with increasing nanoparticle implantation doses. We define an equivalent thickness t_{eq}, as the thickness of the cluster-assembled film resulting from the same amount of implanted nanoparticles deposited on a hard substrate (e.g., glass) (see the Supporting Information). The equivalent thickness for the three different implantation doses investigated was varied in the range 8−15 nm.

Au nanoparticles were implanted to a depth of 70−80 nm below the surface (TEM image, Figure 1c). Such implantation depth, (the thickness of effective skin of nanocomposite AuNPs/PS) is considerably larger than the equivalent thick-

DOI: 10.1021/acsami.5b00825
ACS Appl. Mater. Interfaces 2015, 7, 7060−7065

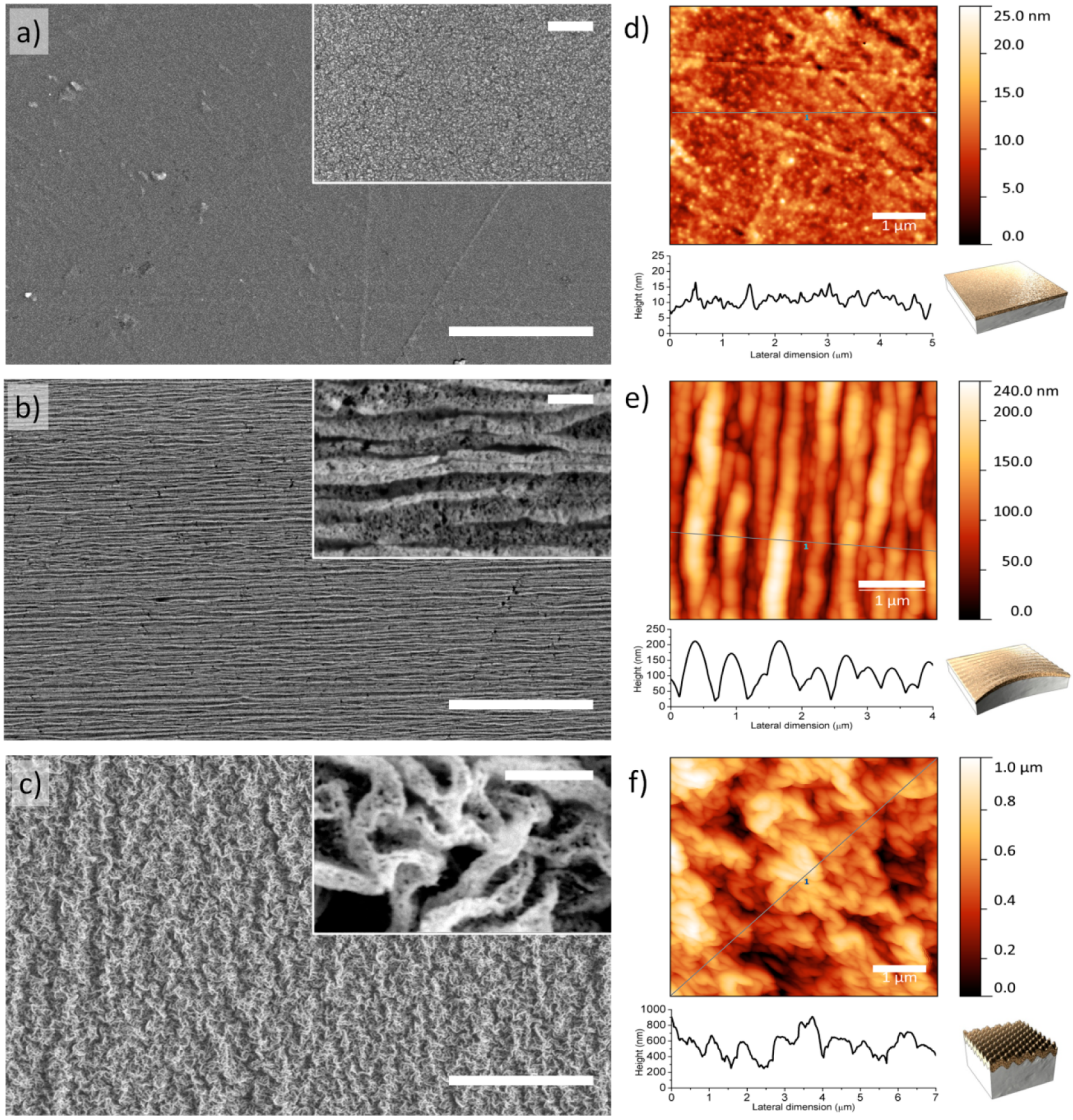

Figure 2. Micronanostructure and topography of nanocomposite with SCB-implanted Au NPs (t_{eq} = 15 nm). SEM images of (a) flat, (b) 1D wrinkled, and (c) 2D wrinkled samples; scale bar 10 μm (magnified inset scale bar 300 nm). AFM imaging and height profiles of (d) flat, (e) 1D wrinkled, and (f) 2D wrinkled samples. Scale bar 1 μm.

ness. Figure 1d shows the same sample after uniaxial shrinking. Along with formation of wrinkles, the implanted skin experienced a rearrangement: the implanted nanoparticles were compacted by compressive forces acting during the thermal shrinkage.

Upon thermal annealing and the subsequent shrinking, we observed the wrinkling of the nanocomposites (Figure 2): investigation of the surface by means of SEM and AFM imaging clearly evidenced the formation of wrinkles with submicrometric spatial periodicity and topographic reliefs over the whole implanted surface.

By comparing samples with identical implantation doses (t_{eq} = 15 ± 2 nm) but different shrinking conditions (no shrink, 1D shrink, 2D shrink) it is possible to appreciate the evolution of wrinkling and how it is affecting sample topography (Figure 2a-f). Interestingly, nanoscale roughness/porosity is evidenced in SEM images at higher magnification (inset of Figure 2b, c), and is related to the size of metal clusters and gaps between adjacent clusters. The superposition of features at different scales, namely the nanostructuring (given by the cluster arrangement of nanocomposite) combined with the microstructuring (driven by wrinkling), is interesting in view of different applications, such as the development of catalytic surfaces for sensing, energy harvesting or also for optics.[23]

We compared wrinkled implanted nanocomposites with Au/PS bilayer with gold layers of similar thickness deposited by sputter coating (no implantation).[10] In the latter case, the "skin" which is subjected to wrinkling is a quite uniform and stiff metal layer that is deformed by compression when the substrate (PS) is heat-shrunk. The gold layer act as a solid barrier which does not permit any flow of the PS (a viscoelastic fluid at at T = 160 °C, that is well above its glass transition temperature T_g ≈ 100 °C) toward the surface; a sharp boundary between PS and wrinkled Au is reported.[10] On the contrary, in our nanocomposite, such mass flow is allowed (especially at low implantation dose), so that wrinkles are well-embedded and partially buried down in PS, as visible in TEM of cross-sections (Figure 1d). As an important implication, incorporation of wrinkled conductive skin in the material causes a very strong adhesion. These observations are further

DOI: 10.1021/acsami.5b00825
ACS Appl. Mater. Interfaces 2015, 7, 7060−7065

confirmed by the AFM profiles reported in Figure 2 e, f: instead of a quasi-sinusoidal profile, as one could expect to be formed by a wrinkling phenomenon, only an half-wave profile is observed, with a peak-to-valley amplitude that is lower than the full amplitude of wrinkles, as observed in TEM images.

By varying the nanoparticle implantation dose, we were able to tune the surface topographical patterns as well as to modulate the electrical conductance G of the nanocomposite. The latter showed an evolution corresponding to a sharp increase (5−6 orders of magnitude) with increasing the implantation dose (Figure 3b), as a result of increased connectivity of implanted conductive particles.[21] Shrinked samples exhibited even better electrical conductivity, with ca. 20−50 times improvement of conductance of 2D wrinkled samples with respect to the flat. Moreover, 1D wrinkled samples showed anisotropic electrical behavior. Conductance measured along perpendicular direction to wrinkles (i.e., the direction on which shrink was allowed during sample preparation) had a similar improvement as observed in 2D samples, while only a ca. 10 times conductance improvement with respect to flat was assessed along parallel direction to wrinkles.

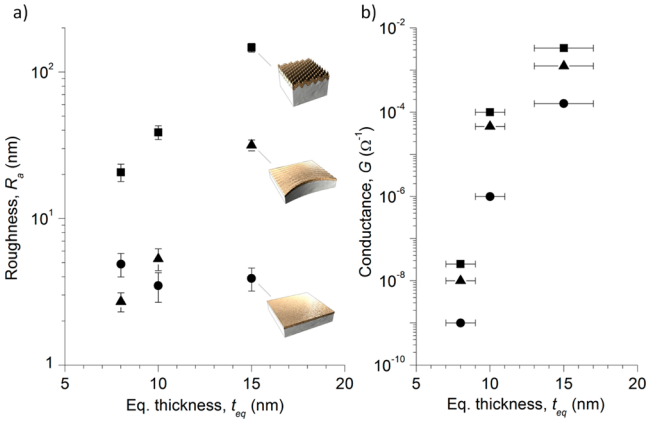

Figure 3. (a) Surface roughness R_a and (b) conductance G of SCB-implanted nanocomposites with different shrinking geometries (flat (not shrunk), circle; 1D wrinkled, triangle; 2D wrinkled, square) as a function of Au NPs t_{eq} (implantation dose).

Average surface roughness R_a of flat (not shrunk) samples, as measured by AFM images analysis, was almost unaffected by increasing the implantation dose. On the other hand, roughness R_a remarkably increased with implantation dose (equivalent thickness) in the case of shrunk nanocomposites, as a result of surface wrinkling (Figure 3a). Noteworthy, by increasing the implantation dose (i.e., the equivalent thickness) no significant change in implantation depth was observed (data not shown); this result is in agreement with previous findings of nanoparticle implantation in PDMS, in which implantation depth was found to be larger (~120 nm), because of its lower modulus, 100 kPa, with respect to polystyrene, 1−2 GPa, and independent of implantation dose.[22]

On the contrary, the observed wrinkling behavior strongly depends upon the implantation dose: as implantation dose was varied ($5 < t_{eq} < 15$ nm) features with distinctly different characteristic size were obtained. A collection of SEM, AFM, and TEM images of samples at all the different t_{eq} and shrinking geometries are reported in the Supporting Information (Figure S1−S3). Noteworthy, the grainlike structure of the nanocomposite made of individual clusters is better emerging in

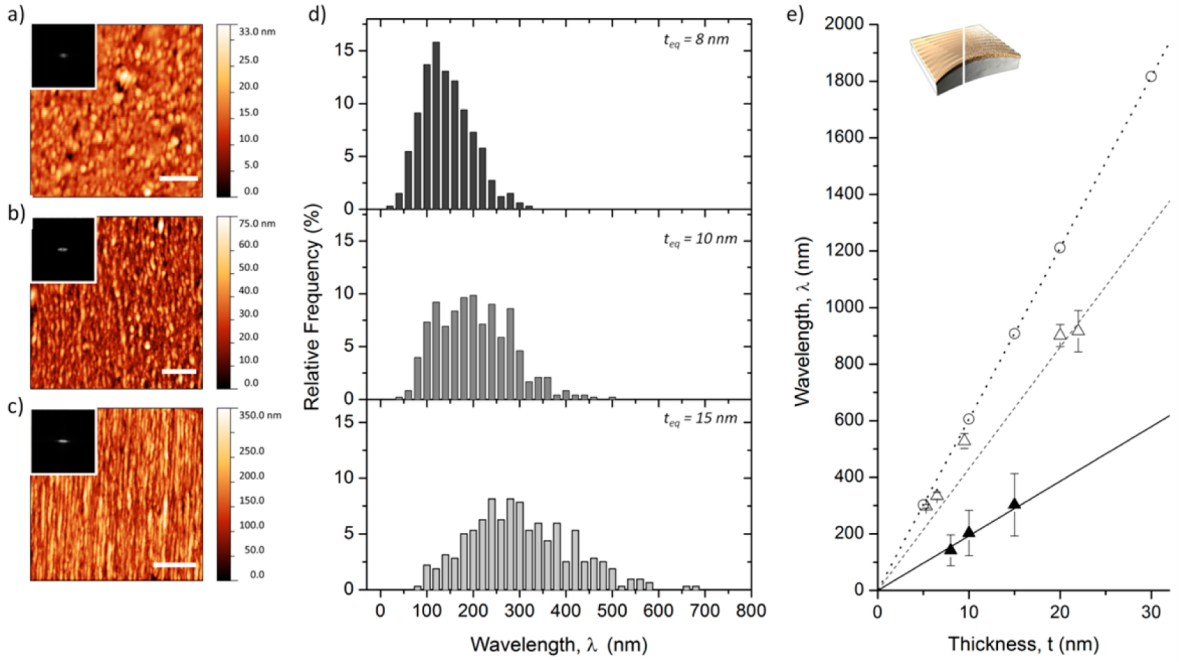

Figure 4. Uniaxially wrinkled (1D) nanocomposites: tunability of surface topography with implantation dose/equivalent thickness of SCB-implanted AuNPs. AFM images and corresponding FFT modulus of 1D samples at different eq thickness: (a) t_{eq} = 8 nm (scale bar 1 μm), (b) t_{eq} = 10 nm (scale bar 2 μm), (c) t_{eq} = 15 nm (scale bar 5 μm). (d) Relative frequency distributions of wrinkle wavelength λ, as estimated by AFM: t_{eq} = 8 nm (top panel), t_{eq} = 10 nm (middle), t_{eq} = 15 nm (bottom). (e) Average wrinkle wavelength λ as a function of t_{eq}: comparison among SCBI Au-NPs composites (black solid triangles), bilayer with sputter-coated Au thin films (open triangles) and theoretical prediction from eq 1 (circles).[2] Linear fits are represented with lines.

DOI: 10.1021/acsami.5b00825
ACS Appl. Mater. Interfaces 2015, 7, 7060−7065

samples at lower t_{eq}, because of the lower amount of implanted AuNPs. To investigate the effects on wrinkling of increasing implantation dose we performed a quantitative analysis on AFM profiles (Figure 4a−c) to evaluate wrinkles alignment and to extract characteristic periodicity (wavelength) of wrinkles in the case of 1D samples. FFT of AFM images (inset of Figure 4a−c) highlight the anisotropic nature of wrinkling with good alignment of wrinkles along vertical direction for all the studied samples. Furthermore, in our analysis, we measured the wavelength λ as the distance between neighboring peaks in the AFM profiles and reconstructed the distribution of measured λ in order to describe heterogeneity of the wrinkling. By increasing the implantation dose the λ distribution broadened and shifted toward larger values (Figure 4d). Notably all the samples were characterized by nanowrinkling with median values of distributions varying from 130 to 300 nm, and distribution ranging from some tens of nanometers (t_{eq} = 8 nm) up to 680 nm (t_{eq} = 15 nm). It is important to notice that such values are among the lowest ever reported for wrinkling.

Deeper insight in these results can be gained by a comparison with experimental results of wrinkling obtained in the case of Au films deposited on top of PS by means of sputter coating (not implanted), and with predictions of a model for wrinkling. By considering the common model that describes wrinkling on an elastic substrate, spatial periodicity of wrinkles along the surface plane (characteristic wavelength λ) is determined solely by the thickness and by intrinsic material properties of the "skin" film and the soft substrate[2]

$$\lambda = 2\pi t\left[\frac{(1-\nu_s^2)E_f}{3(1-\nu_f^2)E_s}\right]^{1/3} \quad (1)$$

where t is the thickness of the film, E is the Young's modulus, ν is the Poisson ratio, f and s subscripts denote film and substrate, respectively.

Figure 4e reports the trend of characteristic λ as a function of nanoparticle equivalent thickness. Values of λ predicted by eq 1 are also reported; the material parameters used in calculation were taken from available literature and were E_f = 60 GPa, ν_f = 0.33 for sputter-coated Au,[24,25] and E_s = 20 MPa, ν_s = 0.45 for PS (at T = 160 °C, that is, the temperature at which shrinking is operated and wrinkles are generated).[26,27]

A remarkable difference in λ is observed between Au implanted nanocomposite and sputter coated Au with similar thickness on top of identical PS substrates. These results further confirm the hypothesis that the effective implanted skin layer has the properties of a nanocomposite. Indeed, by considering eq 1, $\lambda \propto (E_f/E_s)^{1/3}$, wrinkle wavelength depends on intrinsic properties of the materials: the ratio of elastic moduli of film and substrate. Thus, the finding of smaller λ and different slope in the case of implanted AuNPs is an indirect evidence for the formation of a skin layer whose elastic modulus is lower than a continuous Au film and higher than PS. This is in accordance with the behavior of a nanocomposite whose modulus is a combination of moduli of constituent materials. The not perfect accordance of predictions of eq 1 with experimental data found in the case of sputter coated Au samples is explained taking into account several factors: (i) model of eq 1 is based on the assumption of a perfectly elastic substrate, which is not the case for PS (at $T > T_g$) whose behavior is rather affected by viscoelasticity; (ii) data of E and υ taken from literature (Au, PS) must be considered as "order of magnitude" estimate: there are no available data on the materials used in this research, at same thickness; (iii) as regards sputter coated ultrathin Au film, it is known to have a transition in physical properties (elastic modulus, electrical resistivity) exactly in the thickness range of interest (5−15 nm), because of its grain structure and discontinuity during growth, which is completely avoided only at thickness >13−15 nm.[16,24]

In conclusion, we reported the fabrication and characterization of a metal−polymer nanocomposite which creates surface wrinkles at the micro and nanoscale on large areas upon shrinking. Implantation of Au NPs by SCBI in a commercial shrinkable thermoplastic material permitted to avoid its modification upon implantation, thus maintaining the relevant properties of the polymer matrix and of its surface, while imparting electrical conductivity. Surface characterization by means of SEM, AFM, and TEM permitted us to obtain a clear view of wrinkle formation and highlight the relevant differences between such a system and common wrinkled bilayers of metal/polymer. Notably, because of the nanocomposite nature of the implanted "skin", wrinkles are partly buried down into the material. By changing the implantation dose, we were able to follow and to control the corresponding evolution of wrinkling, as well as the electrical conductivity of the nanocomposite. Relevant improvement of conductive properties was observed upon shrink-induced wrinkling, with anisotropic behavior in the case of aligned wrinkles. The combination of features at the nanoscale and at hundreds of nanometer scale of the nanocomposite and the possibility to tune them by changing the amount of implanted nanoparticles are unique and they could open the way to several applications requiring multiscale integration and organization of periodic structures in the field of optics, biointerfacing, sensing, and microfabrication.

■ ASSOCIATED CONTENT

Supporting Information

Details about experimental procedures. Figures S1−S4, reporting SEM, AFM, and TEM images of all samples investigated in dependence of implantation dose and shrinking geometry. This material is available free of charge via the Internet at http://pubs.acs.org.

■ AUTHOR INFORMATION

Corresponding Authors

*E-mail: francesco.greco@iit.it.
*E-mail: paolo.milani@mi.infn.it.

Notes

The authors declare no competing financial interest.

■ ACKNOWLEDGMENTS

The authors acknowledge Paola Parlanti for assistance during the cutting process.

■ REFERENCES

(1) Groenewold, J. Wrinkling of Plates Coupled with Soft Elastic Media. *Phys. A* **2001**, *298*, 32−45.
(2) Genzer, J.; Groenewold, J. Soft Matter with Hard Skin: From Skin Wrinkles to Templating and Material Characterization. *Soft Matter* **2006**, *2*, 310−323.
(3) Bowden, N.; Brittain, S.; Evans, A. G.; Hutchinson, J. W.; Whitesides, G. M. Spontaneous Formation of Ordered Structures in Thin Films of Metals Supported on an Elastomeric Polymer. *Nature* **1998**, *393*, 146−149.

DOI: 10.1021/acsami.5b00825
ACS Appl. Mater. Interfaces 2015, 7, 7060−7065

(4) Cerda, E.; Ravi-Chandar, K.; Mahadevan, L. Thin Films: Wrinkling of an Elastic Sheet under Tension. *Nature* **2002**, *419*, 579−580.
(5) Huck, W. T. S.; Bowden, N.; Onck, P.; Pardoen, T.; Hutchinson, J. W.; Whitesides, G. M. Ordering of Spontaneously Formed Buckles on Planar Surfaces. *Langmuir* **2000**, *16*, 3497−3501.
(6) Efimenko, K.; Rackaitis, M.; Manias, E.; Vaziri, A.; Mahadevan, L.; Genzer, J. Nested Self-Similar Wrinkling Patterns in Skins. *Nat. Mater.* **2005**, *4*, 293−297.
(7) Chen, C. M.; Yang, S. Wrinkling Instabilities in Polymer Films and Their Applications. *Polym. Int.* **2012**, *61*, 1041−1047.
(8) Mei, Y.; Kiravittaya, S.; Harazim, S.; Schmidt, O. G. Principles and Applications of Micro and Nanoscale Wrinkles. *Mater. Sci. Eng., R* **2010**, *70*, 209−224.
(9) Stafford, C. M.; Harrison, C.; Beers, K. L.; Karim, A.; Amis, E. J.; VanLandingham, M. R.; Kim, H.-C.; Volksen, W.; Miller, R. D.; Simonyi, E. E. A Buckling-Based Metrology for Measuring the Elastic Moduli of Polymeric Thin Films. *Nat. Mater.* **2004**, *3*, 545−550.
(10) Fu, C. C.; Grimes, A.; Long, M.; Ferri, C. G. L.; Rich, B. D.; Ghosh, S.; Lee, L. P.; Gopinathan, A.; Khine, M. Tunable Nanowrinkles on Shape Memory Polymer Sheets. *Adv. Mater.* **2009**, *21*, 4472−4476.
(11) Fu, C. C.; Ossato, G.; Long, M.; Digman, M. A.; Gopinathan, A.; Lee, L. P.; Gratton, E.; Khine, M. Bimetallic Nanopetals for Thousand-Fold Fluorescence Enhancements. *Appl. Phys. Lett.* **2010**, *97*, 203101.
(12) Sharma, H.; Digman, M. A.; Felsinger, N.; Gratton, E.; Khine, M. Enhanced Emission of Fluorophores on Shrink-Induced Wrinkled Composite Structures. *Opt. Mater. Express* **2014**, *4*, 753−763.
(13) Chen, A.; Lieu, D. K.; Freschauf, L.; Lew, V.; Sharma, H.; Wang, J.; Nguyen, D.; Karakikes, I.; Hajjar, R. J.; Gopinathan, A.; Botvinick, E.; Fowlkes, C. C.; Li, R. A.; Khine, M. Shrink-Film Configurable Multiscale Wrinkles for Functional Alignment of Human Embryonic Stem Cells and Their Cardiac Derivatives. *Adv. Mater.* **2011**, *23*, 5785−5791.
(14) Freschauf, L. R.; McLane, J.; Sharma, H.; Khine, M. Shrink-Induced Superhydrophobic and Antibacterial Surfaces in Consumer Plastics. *PLoS One* **2012**, *7*, e40987.
(15) Greco, F.; Ventrelli, L.; Dario, P.; Mazzolai, B.; Mattoli, V. Micro-Wrinkled Palladium Surface for Hydrogen Sensing and Switched Detection of Lower Flammability Limit. *Int. J. Hydrogen Energy* **2012**, *37*, 17529−17539.
(16) Greco, F.; Fujie, T.; Ricotti, L.; Taccola, S.; Mazzolai, B.; Mattoli, V. Microwrinkled Conducting Polymer Interface for Anisotropic Multicellular Alignment. *ACS Appl. Mater. Interfaces* **2013**, *5*, 573−584.
(17) Leser, M.; Pegan, J.; El Makkaoui, M.; Schlatterer, J. C.; Khine, M.; Law, M.; Brenowitz, M. Protein Footprinting by Pyrite Shrink-Wrap Laminate. *Lab Chip* **2015**, *15*, 1646−1650.
(18) Hammock, M. L.; Chortos, A.; Tee, B. C. K.; Tok, J. B. H.; Bao, Z. 25th Anniversary Article: The Evolution of Electronic Skin (E-Skin): A Brief History, Design Considerations, and Recent Progress. *Adv. Mater.* **2013**, *25*, 5997−6038.
(19) Bauer, S.; Bauer-Gogonea, S.; Graz, I.; Kaltenbrunner, M.; Keplinger, C.; Schwödiauer, R. 25th Anniversary Article: A Soft Future: From Robots and Sensor Skin to Energy Harvesters. *Adv. Mater.* **2014**, *26*, 149−162.
(20) Ravagnan, L.; Divitini, G.; Rebasti, S.; Marelli, M.; Piseri, P.; Milani, P. Poly(Methyl Methacrylate)-Palladium Clusters Nanocomposite Formation by Supersonic Cluster Beam Deposition: A Method for Microstructured Metallization of Polymer Surfaces. *J. Phys. D: Appl. Phys.* **2009**, *42*, 082002.
(21) Corbelli, G.; Ghisleri, C.; Marelli, M.; Milani, P.; Ravagnan, L. Highly Deformable Nanostructured Elastomeric Electrodes with Improving Conductivity Upon Cyclical Stretching. *Adv. Mater.* **2011**, *23*, 4504−4508.
(22) Ghisleri, C.; Borghi, F.; Ravagnan, L.; Podestà, A.; Melis, C.; Colombo, L.; Milani, P. Patterning of Gold-Polydimethylsiloxane (Au-Pdms) Nanocomposites by Supersonic Cluster Beam Implantation. *J. Phys. D: Appl. Phys.* **2014**, *47*, 015301.
(23) Zhang, L.; Lang, X.; Hirata, A.; Chen, M. Wrinkled Nanoporous Gold Films with Ultrahigh Surface-Enhanced Raman Scattering Enhancement. *ACS Nano* **2011**, *5*, 4407−4413.
(24) Salvadori, M.; Brown, I.; Vaz, A.; Melo, L.; Cattani, M. Measurement of the Elastic Modulus of Nanostructured Gold and Platinum Thin Films. *Phys. Rev. B: Condens. Matter Mater. Phys.* **2003**, *67*, 153404.
(25) Cao, C.; Chan, H. F.; Zang, J.; Leong, K. W.; Zhao, X. Harnessing Localized Ridges for High-Aspect-Ratio Hierarchical Patterns with Dynamic Tunability and Multifunctionality. *Adv. Mater.* **2014**, *26*, 1763−1770.
(26) Gedde, U. *Polymer Physics*; Springer: New York, 1995.
(27) Mott, P. H.; Dorgan, J. R.; Roland, C. M. The Bulk Modulus and Poisson's Ratio of "Incompressible" Materials. *J. Sound Vibration* **2008**, *312*, 572−575.

DOI: 10.1021/acsami.5b00825
ACS Appl. Mater. Interfaces 2015, 7, 7060−7065